

# Computational and Spectroscopic Studies on the Formation of Halogen-Bonded Complexes Between Tertiary Amines and CBr<sub>4</sub> and Application in the Light-Mediated Amino Acid Coupling

E. Alexandros Routsis<sup>+</sup>,<sup>[a, b]</sup> Christiana Mantzourani<sup>+</sup>,<sup>[a, b]</sup> Marie Rrapi,<sup>[a, b]</sup> Olga G. Mountanea,<sup>[a, b]</sup> Maroula G. Kokotou,<sup>\*,[c]</sup> Demeter Tzeli,<sup>\*,[d, e]</sup> Christoforos G. Kokotos,<sup>[a, b]</sup> and George Kokotos<sup>\*,[a, b]</sup>

In recent years, halogen-bonded complexes (XBCs), in solution, have played a pivotal role in inducing photochemical organic reactions. In this work, we explore the ability of various tertiary amines to act as XB acceptors in the presence of the XB donor CBr<sub>4</sub> by computational and spectroscopic studies. DFT studies clearly showcase the formation of XBCs between the studied tertiary amines and CBr<sub>4</sub>. Simultaneously, computational and experimental UV-Vis studies display intense red shifts that are consistent with charge transfer observed from tertiary amines to CBr<sub>4</sub>. A detailed NMR study revealed a clear chemical shift of the carbon carrying the bromine atoms upon mixing the XB

acceptor with the donor, suggesting that this spectroscopic technique is indeed an experimental tool to identify the generation of XBCs. An application of the ability of such XBCs to activate a carboxylic acid under UVA irradiation or sunlight is presented for amino acid coupling. Among the various tertiary amines studied, the pair DABCO-CBr<sub>4</sub> was found to work well for the photochemical amide bond formation. Direct infusion-HRMS studies allowed us to propose a general mechanism for the photochemical amino acid coupling in the presence of a tertiary amine and CBr<sub>4</sub>, initiated by the photoactivation of an XBC.

## Introduction

Halogen atoms (X) are usually considered as electronegative reactive species that participate in non-covalent interactions by functioning as electron donor sites. However, the electron density in X is anisotropically distributed, whenever they are covalently bound to other atoms in compounds. This phenomenon results in two regions of electron density: a region of higher electron density, the origin of many typical interactions that X are involved in, and a region of depleted electron density ( $\sigma$ -hole), which has the ability to form attractive interactions with electron-rich sites, such as nucleophiles. Halogen bonding fits in this category.<sup>[1a]</sup>

Halogen bonding (XB) refers to non-covalent interactions of halogen atoms with electron-rich species, such as lone pair electrons of Lewis bases (N, O, S, P) and p electron donors.<sup>[1]</sup> These interactions are based on the existence of  $\sigma$ -holes, which represent the region of positive electrostatic potential of the covalent-bonded X. The  $\sigma$ -hole is able to interact with negative sites on other molecules, leading to the formation of halogen-bonded complexes (XBCs). The electron density transfer resulting from XB between the  $\sigma$ -hole of X in a RX molecule (XB donor) and a Lewis base Y (XB acceptor) results in shortening of the interatomic distance of the participating atoms (RX–Y) below the sum of their van der Waals radii, while the R–X bond is elongated (Figure 1).<sup>[1b]</sup> Some of the features of XB include a

[a] E. A. Routsis,<sup>+</sup> Dr. C. Mantzourani,<sup>+</sup> M. Rrapi, O. G. Mountanea, Prof. Dr. C. G. Kokotos, Prof. Dr. G. Kokotos  
Laboratory of Organic Chemistry, Department of Chemistry, National and Kapodistrian University of Athens,  
Panepistimiopolis, Athens 15771, Greece  
E-mail: gkokotos@chem.uoa.gr

[b] E. A. Routsis,<sup>+</sup> Dr. C. Mantzourani,<sup>+</sup> M. Rrapi, O. G. Mountanea, Prof. Dr. C. G. Kokotos, Prof. Dr. G. Kokotos  
Center of Excellence for Drug Design and Discovery, National and Kapodistrian University of Athens, Athens 15771, Greece

[c] Prof. Dr. M. G. Kokotou  
Laboratory of Chemistry, Department of Food Science and Human Nutrition,  
Agricultural University of Athens, Iera Odos 75, Athens 11855, Greece  
E-mail: mkokotou@aua.gr

[d] Prof. Dr. D. Tzeli  
Laboratory of Physical Chemistry, Department of Chemistry,  
National and Kapodistrian University of Athens,  
Panepistimiopolis Athens 15771, Greece  
E-mail: tzeli@chem.uoa.gr

[e] Prof. Dr. D. Tzeli  
Theoretical and Physical Chemistry Institute,  
National Hellenic Research Foundation,  
48 Vassileos Constantinou Ave., Athens 11635, Greece

[<sup>+</sup>] These authors contributed equally

Supporting information for this article is available on the WWW under <https://doi.org/10.1002/cplu.202400019>

© 2024 The Authors. ChemPlusChem published by Wiley-VCH GmbH. This is an open access article under the terms of the Creative Commons Attribution Non-Commercial License, which permits use, distribution and reproduction in any medium, provided the original work is properly cited and is not used for commercial purposes.

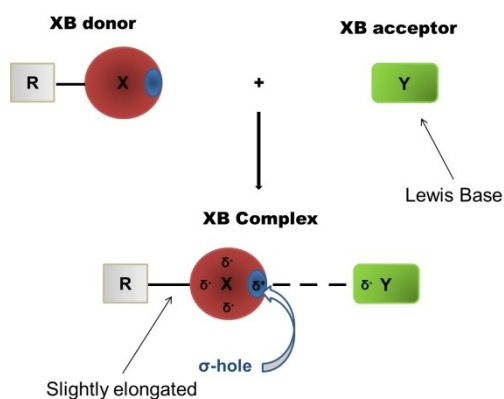


**Figure 1.** Schematic representation of the formation of a halogen-bonded complex between an XB donor and an XB acceptor.

preference for  $180^\circ$  R–X–Y angles and an increase in its strength for the heavier halogens ( $R-F < R-Cl < R-Br < R-I$ ), since high electron-attracting Xs, such as F, tend to neutralize the  $\sigma$ -hole.<sup>[1c,d]</sup> However, recently, Bickelhaupt *et al.* have stated that the  $\sigma$ -hole model is incorrect and does not allow for a correct understanding of the nature of halogen bonds.<sup>[2]</sup> Their quantum analyses indicated that electrostatic interactions, on which the  $\sigma$ -hole is based on, favor bending and not directionality, a fact that completely contradicts the  $\sigma$ -hole model's principles. Instead, they claimed that directionality is attributed to the minimization of Pauli repulsion between the lone pair orbitals of the acceptor and the occupied p atomic orbitals of the halogen atom.<sup>[2]</sup>

Although XB has been intensively investigated in condensed phases in crystal engineering, only recently there have been studies in solution, especially for applications in Organic Synthesis.<sup>[1b,c]</sup> XBCs are important tools in Organocatalysis and Asymmetric Catalysis, since they can induce a variety of organic transformations, such as halogenation, cyclopropanation, Ritter reaction, Diels–Alder reaction, Aza–Diels–Alder reaction, Morita–Baylis–Hillman reaction and Michael reaction etc.<sup>[1d,3]</sup> Nowadays, there have also been multiple studies for the catalytic formation of C-centered radicals, useful intermediates, via visible-light-initiated reactions, based on the principles of Photoorganocatalysis, a promising branch in Organic Chemistry. These transformations rely on photoactivation of XBCs, for the generation of C-centered radicals.<sup>[4]</sup>

Recently, carbon tetrabromide ( $CBr_4$ ) has been intensively utilized as a XB donor in various organic transformations, such as the synthesis of  $\alpha,\beta$ -unsaturated ketones via selective activation of benzaldehyde,<sup>[5a]</sup> the three-component reactions of aldehydes, amines and diethylphosphite for the synthesis of  $\alpha$ -amino phosphonates, under solvent-free conditions,<sup>[5b]</sup> the formation of C–S bonds,<sup>[5c]</sup> the acylation of phenols, alcohols, and thiols,<sup>[5d]</sup> etc. The existing literature extensively documents the investigation into the interaction between XB donors, especially  $CBr_4$ , and diverse XB acceptors. Notably, studies in this field have given particular attention to employing computation and UV–Vis spectroscopy, providing an insightful analysis of electronic transitions and structural alterations that take

place during the formation of XBCs.<sup>[5a,6]</sup> In 1987, Kochi *et al.* conducted a study on the molecular interaction between various amines and tetrahalomethanes, emphasizing spectroscopic analysis with a focus on observing charge-transfer (CT) absorption bands.<sup>[6b]</sup> Particularly noteworthy was the observation that when DABCO was introduced to  $CBr_4$  and UV–Vis spectra were recorded, a distinct broad shoulder peak became evident. This effect was further accentuated with extra addition of the base to  $CBr_4$ .<sup>[6b]</sup> Similar results were found in a study by Yamaguchi and Itoh, investigating  $CBr_4$ 's interaction with a different base, specifically 4-phenylpyridine.<sup>[6h]</sup> The UV–Vis spectrum of an equimolar mixture of 4-phenylpyridine with  $CBr_4$  displayed a new absorption band at 444 nm, indicating the formation of a charge-transfer complex (CTC). Experimental evidence indicated a concentration-dependent red-shifted shoulder on  $CBr_4$ , suggesting XB interactions between  $CBr_4$  and 4-phenylpyridine. This observation likely indicates CT-initiated catalysis between 4-phenylpyridine and  $CBr_4$ , followed by photoexcitation to generate the active species.<sup>[6h]</sup>

The formation of an amide bond is of high importance and it finds wide applications both in academia and industry.<sup>[7]</sup> The majority of the methods used for the synthesis of amides and peptides employ coupling reagents,<sup>[8]</sup> which are usually expensive and sometimes require tedious preparation. Following the revolutionary breakthrough of novel light-mediated organic transformations, several photochemical methods for the amide bond formation have been reported, employing a variety of starting materials.<sup>[9]</sup> However, only a few of them demonstrate the direct coupling of carboxylic acids or derivatives to amines under irradiation.<sup>[10]</sup>

In 2021, Szpilman *et al.* demonstrated the coupling of amino acids using 4-dimethylaminopyridine (DMAP) and  $BrCCl_3$  under solar irradiation.<sup>[10d]</sup> Recently, we have presented the synthesis of Weinreb and morpholine amides from carboxylic acids using DMAP– $BrCCl_3$  either under sunlight or LED 370 nm irradiation.<sup>[11]</sup> In addition, we have demonstrated the coupling of carboxylic acids with protected hydroxylamines for the synthesis of various hydroxamic acids, using the same combination of reagents either under sunlight or LED 370 nm irradiation.<sup>[12]</sup> Most recently, we have reported the photochemical amidation reaction using pyridine– $CBr_4$  under UVA irradiation via a novel carboxylic acid photoactivation mode, involving the generation of a symmetric anhydride intermediate.<sup>[13]</sup>

As proposed by Szpilman *et al.* in their protocol,<sup>[10d]</sup> the mechanism of the amide synthesis involves the formation of a CTC between DMAP and  $BrCCl_3$  as the first step, which upon sunlight irradiation and photoactivation generates a novel coupling reagent *in situ*. They speculated the formation of a hemiaminal ester as the key-intermediate.<sup>[10d]</sup> In our photochemical protocol for the synthesis of Weinreb and morpholine amides, as well as in the coupling of carboxylic acids to protected hydroxylamines, we were able to detect by High Resolution Mass Spectrometry (HRMS) the generation of ions corresponding to the hemiaminal ester of the corresponding carboxylic acid, providing experimental evidence for its formation.<sup>[11,12]</sup>

The aim of the present work was to study the formation of XBCs between various tertiary amines (XB acceptors) and  $\text{CBr}_4$  (XB donor) in solution, employing computational and spectroscopic approaches, and to explore an application of such XBCs in light-mediated reactions. To define the ability of each tertiary amine and  $\text{CBr}_4$  to generate an XBC, DFT studies were carried out to calculate the binding energy between  $\text{CBr}_4$  and each XB acceptor and the geometry of the involved singlet ground states and first excited triplet states. UV-Vis spectroscopy was used as an established experimental tool to demonstrate the generation of CTCs via halogen bonding. Furthermore, we demonstrate that  $^{13}\text{C}$ -NMR spectroscopy is an additional experimental technique to easily understand the generation of XB. An application of XBCs between tertiary amines and  $\text{CBr}_4$  in light-mediated reactions, across various wavelengths, was studied for an amino acid coupling reaction, driven by the hypothesis that aligning the experimental results with absorption bands might reveal an enhancement in the reaction yield, particularly in proximity to the wavelength associated with the red-shifted shoulder. Finally, the reaction mechanism of such a light-mediated coupling was extensively studied, using HRMS as the key-tool.

## Results and Discussion

Although the mechanism of the light-mediated DMAP- $\text{BrCCl}_3$  amide bond synthesis begins with the formation of a XBC via

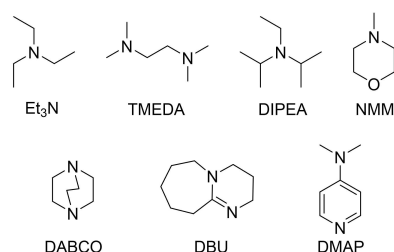


**Figure 2.** Tertiary amines studied in the present work for their ability to generate XBCs with  $\text{CBr}_4$ .

the pyridine nitrogen of DMAP, the essential hemiaminal ester intermediate is formed via its tertiary nitrogen.<sup>[10d]</sup> We envisioned, that in general a tertiary amine could play a dual role, both acting as an XB acceptor and offering the possibility to generate a hemiaminal ester intermediate. As a matter of fact, it has been known since the sixties, that some tertiary amines are able to form XBCs with halomethanes.<sup>[6]</sup> Triethylamine ( $\text{Et}_3\text{N}$ ) has been shown to form complexes with halomethanes, such as  $\text{CCl}_4$ ,  $\text{BrCCl}_3$  or  $\text{CBr}_4$ ,<sup>[6a]</sup> while quinuclidine or 1,4-diazabicyclo[2.2.2]octane (DABCO) have been demonstrated to form crystal structures with  $\text{CBr}_4$ .<sup>[6b]</sup> The last complex is characterized by its CT absorption band and its irradiation leads to the formation of  $\text{CBr}_4$  anion radical<sup>[6f]</sup> and DABCO cation radicals, which then participate in the follow-up reactions.<sup>[6b]</sup> Thus, in the present work, we explored the ability of several tertiary amines to form XBCs with  $\text{CBr}_4$ . The amines used, namely  $\text{Et}_3\text{N}$ , tetramethylethylenediamine (TMEDA), *N,N*-diisopropylethylamine (DIPEA), *N*-methylmorpholine (NMM), DABCO and 1,8-diazabicyclo[5.4.0]undec-7-ene (DBU), are depicted in Figure 2. DMAP, which has been previously studied by us for its interaction with  $\text{CBr}_4$ ,<sup>[13]</sup> was also included for comparison purposes.

Occasionally, computational and spectroscopic studies have been conducted for the case of various amines and haloforms or *N*-haloimides.<sup>[14]</sup> In this study, in order to explore the generation of XBCs between  $\text{CBr}_4$  and DABCO or other tertiary amines, and their properties, DFT studies ( $\omega\text{B97X-D}^{[15]}$ /def2-TZVP,<sup>[16]</sup> in acetonitrile (ACN) as the solvent) were performed. Conformational analysis was carried out at first for all species. For the calculation of the  $S_0$  state of the XBCs, the  $\text{CBr}_4$  molecule was set in different positions around the six calculated amines and the geometries were energetically optimized. Regarding TMEDA, the bidentate coordination of the two N atoms of TMEDA with the Br atom of the  $\text{CBr}_4$  molecule, was investigated, however the geometry optimization studies led to the 2<sup>nd</sup> conformer of the TMEDA- $\text{CBr}_4$  complex (Figure 3), where the Br atom favors in interacting with only one N atom. The lowest in energy conformers are depicted in Figure 3 (for details, see Supporting Information).<sup>[17]</sup> The binding electronic energies, enthalpies and free energies ( $\Delta E_{\text{bind}}$ ,  $\Delta H_{\text{bind}}$ ,  $\Delta G_{\text{bind}}$  respectively)

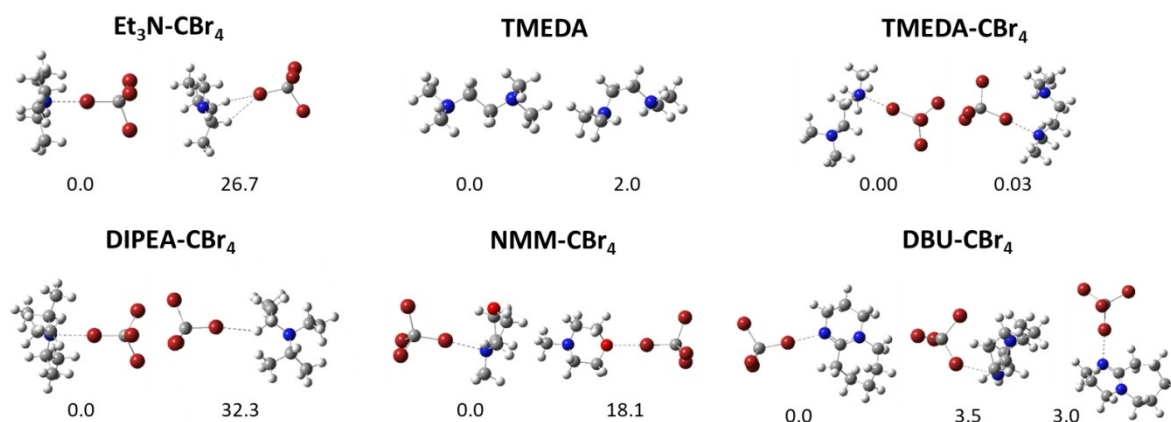


**Figure 3.** Relative energy ordering of the two or three lowest in energy conformers (kJ/mol) of  $\text{Et}_3\text{N}-\text{CBr}_4$ , TMEDA, TMEDA- $\text{CBr}_4$ , DIPEA- $\text{CBr}_4$ , NMM- $\text{CBr}_4$  and DBU- $\text{CBr}_4$ .

between  $\text{CBr}_4$  and each tertiary amine were calculated (Table 1). Negative values of  $\Delta E_{\text{bind}}$  were observed in all cases (Table 1), meaning there are indeed interactions between  $\text{CBr}_4$  and amines.

The strongest binding energy was observed for the DABCO- $\text{CBr}_4$  pair at  $-6.6$  kcal/mol, while the weakest one was found for the previously reported DMAP- $\text{CBr}_4$  at  $-4.4$  kcal/mol<sup>[13]</sup> (Table 1). Additionally, all  $\Delta H_{\text{bind}}$  values were also negative, concluding to the fact that XBC generation is an exothermic process, while  $\Delta G_{\text{bind}}$  values are positive at 298.15 K, due to entropy. All data in Table 1 suggest that all XBCs may be in rapid dynamic equilibrium with their components at room temperature, similarly to DMAP- $\text{BrCCl}_3$  complex that was previously reported by Szpilman *et al.*<sup>[10d]</sup>

Along with the ground states ( $S_0$ , singlet, XBC formation), the lowest in energy triplet states ( $T_1$ , first excited triplet state) of the XBCs were also calculated. Their structures are depicted in Figure 4 and selected geometries are summarized in Table S1.<sup>[17]</sup> In the singlet states, a weak  $\text{Br}\cdots\text{N}$  bond is formed, since the computed distances are shorter than the sum of the vdW radii of the atoms ( $d_{\text{N-Br}} = 3.40$  Å). The C–Br bond of  $\text{CBr}_4$  is

slightly elongated and the C–Br $\cdots$ N angle is almost linear, indicating the formation of halogen bonds. The highest value of the Br $\cdots$ N bond length was observed for the DIPEA- $\text{CBr}_4$  complex at 3.1 Å, probably due to stereochemical restrictions resulting from the neighboring groups. In the computed triplet states, the C–Br bond has been cleaved and the  $\cdot\text{CBr}_3$  radical has been formed. In most cases, the Br atom is connected to the nitrogen, the Br $\cdots$ N bond becomes significantly shorter, especially in the cases of DMAP and DBU complexes, where the decrease is at about 0.3 Å and 0.2 Å, respectively. On the contrary, in the case of the DIPEA- $\text{CBr}_4$  complex, the Br $\cdots$ N bond is elongated by 0.6 Å. Additionally, the CNCC dihedral angles, where the  $\text{sp}^3$  hybridized N atoms of DABCO, DIPEA, NMM,  $\text{Et}_3\text{N}$  and TMEDA interact with the Br atom of  $\text{CBr}_4$ , were calculated in both  $S_0$  and  $T_1$  states. It is obvious that their CNCC dihedral angles increase from  $S_0$  to  $T_1$  state, especially in the case of DIPEA- $\text{CBr}_4$  complex, where the CNCC dihedral angle increases from 129.7 to 163.0 degrees,<sup>[17]</sup> a fact that may be associated with significant shifts in their absorption spectra.<sup>[18]</sup> It should be noted that additional calculations employing the B3LYP-D3,<sup>[19]</sup> M06-2X<sup>[20]</sup> and PBE0<sup>[21]</sup> functionals were carried out, in conjunction with the def2-TZVP basis set for the case of TMEDA- $\text{CBr}_4$ . It was found that all methodologies led to the same minimum structure, indicating the XBC generation. All predict a C–Br $\cdots$ N angle of about 179 degrees in the  $S_0$  state, i.e., a linear halogen bond. The  $\omega\text{B97X-D/def2-TZVP}$  Br $\cdots$ N bond distance is 2.766 Å ( $S_0$ ) and 2.623 Å ( $T_1$ ). The corresponding calculated values with M06-2X/def2-TZVP and B3LYP-D3/def2-TZVP methodologies differ less than 0.1 Å, while the PBE0 values differ less than 0.2 Å (Table S2, Supporting Information).<sup>[17]</sup> Both  $\omega\text{B97X-D}$  and M06-2X predict a shortening of the Br $\cdots$ N bond from the  $S_0$  to the  $T_1$  state, while B3LYP-D3 and PBE0 predict an elongation.<sup>[17]</sup> Overall, all functionals present similar geometries, while the selected used functional,  $\omega\text{B97X-D}$ , is appropriate for the calculation of both short- and long-range interactions such as XB.<sup>[15]</sup>

Regarding the singlet-triplet excitation energies, the computed adiabatic  $S_0 \rightarrow T_1$   $\Delta E_a$  vary from 25 kcal/mol to 31 kcal/mol,  $\Delta H_a$  from 25 kcal/mol to 30 kcal/mol, and  $\Delta G_a$  from 21 kcal/mol to 35 kcal/mol (Table 2), concluding to the fact that the formation of their first excited triplet states is feasible under UVA irradiation.

**Table 1.** Calculated theoretical binding energies  $\Delta E$ , binding enthalpies  $\Delta H$ , and binding Gibbs free energies  $\Delta G$  (all in kcal mol<sup>−1</sup>) of all halogen-bonded complexes in ACN solvent at the  $\omega\text{B97X-D/def2-TZVP}$  methodology.

XB Acceptors	XB Donor $\text{CBr}_4$		
	$\Delta E_{\text{bind}}$	$\Delta H_{\text{bind}}$	$\Delta G_{\text{bind}}$
$\text{Et}_3\text{N}$	−5.8	−4.8	5.7
TMEDA	−6.5	−4.9	2.4
DIPEA	−5.7	−4.1	4.0
NMM	−6.4	−5.5	4.5
DABCO	−6.6	−5.1	2.3
DBU	−5.9	−4.5	1.1
DMAP	−4.4 <sup>[13]</sup>	−3.7	5.2

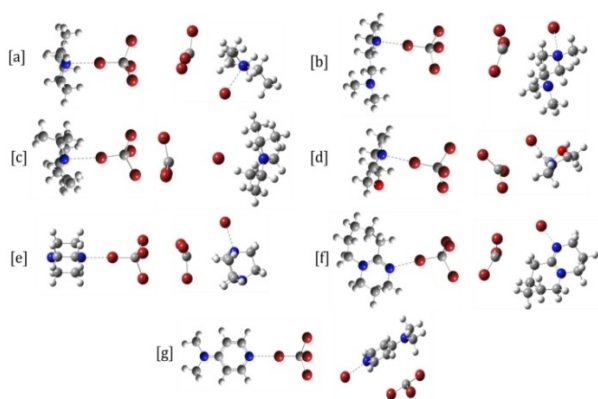


**Figure 4.** Calculated minimum structures of the XBCs (left) and their first excited triplet states (right) at the  $\omega\text{B97X-D/def2-TZVP}$  method; calculated Br $\cdots$ N bond lengths: a.  $\text{Et}_3\text{N-CBr}_4$  ( $S_0$ : 2.803 Å,  $T_1$ : 2.726 Å), b.  $\text{TMEDA-CBr}_4$  ( $S_0$ : 2.766 Å,  $T_1$ : 2.623 Å), c.  $\text{DIPEA-CBr}_4$  ( $S_0$ : 3.068 Å,  $T_1$ : 3.673 Å), d.  $\text{NMM-CBr}_4$  ( $S_0$ : 2.785 Å,  $T_1$ : 2.643 Å), e.  $\text{DABCO-CBr}_4$  ( $S_0$ : 2.678 Å,  $T_1$ : 2.603 Å), f.  $\text{DBU-CBr}_4$  ( $S_0$ : 2.708 Å,  $T_1$ : 2.505 Å), g.  $\text{DMAP-CBr}_4$  ( $S_0$ : 2.773 Å,  $T_1$ : 2.470 Å).<sup>[13]</sup>

**Table 2.** Calculated vertical ( $\Delta E_v$ ) and adiabatic ( $\Delta E_a$ ) singlet-triplet excitation energies ( $S_0 \rightarrow T_1$ ), adiabatic excitation enthalpies ( $\Delta H_a$ ) and adiabatic Gibbs free energies ( $\Delta G_a$ ) in kcal mol<sup>−1</sup> of all XBCs in ACN solvent at the  $\omega\text{B97X-D/def2-TZVP}$  level of theory.

XBC	$\Delta E_v$	$\Delta E_a$	$\Delta H_a$	$\Delta G_a$
$\text{Et}_3\text{N-CBr}_4$	96.2	24.8	25.4	20.6
$\text{TMEDA-CBr}_4$	97.7	26.0	26.2	24.6
$\text{DIPEA-CBr}_4$	95.0	26.7	27.0	21.9
$\text{NMM-CBr}_4$	97.6	27.9	28.5	22.3
$\text{DABCO-CBr}_4$	92.9	26.1	26.2	23.6
$\text{DBU-CBr}_4$	98.0	30.2	30.3	29.3
$\text{DMAP-CBr}_4$	87.3 <sup>[13]</sup>	31.2 <sup>[13]</sup>	27.9	35.3



Furthermore, the UV-Vis absorption spectra of the optimized structures of the XBCs were calculated in ACN as the solvent (Figure 5, left). For comparison purposes and selection of the best methodology for the calculation of the UV-Vis spectra, the UV-Vis absorption spectra of TMEDA,  $\text{CBr}_4$  and  $\text{TMEDA-CBr}_4$  were calculated via the TD- $\omega$ B97X-D/def2-TZVP (Time-Dependent),<sup>[22]</sup> TDA- $\omega$ B97X-D/def2-TZVP (Tamm-Dancoff approximation)<sup>[23]</sup> and TDA-B3LYP/def2-TZVP methods (Figure S1).<sup>[17]</sup> The TD- $\omega$ B97X-D/def2-TZVP and TDA- $\omega$ B97X-D/def2-TZVP methodologies predict very small shifts of about 4 nm,<sup>[17]</sup> while TDA-B3LYP/def2-TZVP predicts a significant red shift of 100–140 nm. Thus, we concluded that the TDA-B3LYP/def2-TZVP method is appropriate for the calculation of the UV-Vis spectra of all XBCs. Note that TDA-B3LYP/def2-TZVP level of theory was employed at the  $S_0$  optimized geometries, obtained via the  $\omega$ B97X-D/def2-TZVP method.

The  $\lambda$  (nm) values of the  $S_0 \rightarrow S_1$  excitation and of the main peaks of the absorption spectra of XBCs in ACN as the solvent are given in Table S3.<sup>[17]</sup> The computed UV-Vis spectra clearly indicate that CT, as a result of halogen bonding, causes the red shifts, since new peaks appear at around 355–440 nm, compared to their components (Figure 5, left). The peaks corresponding to the  $S_0 \rightarrow S_1$  excitation of the XBCs complexes are observed in the area that range from 354 nm (NMM- $\text{CBr}_4$ ) to 441 nm (DABCO- $\text{CBr}_4$ ). These peaks result from H $\rightarrow$ L molecular orbital excitations, where in all studied complexes, charge transfers are observed from the HOMO orbitals of the XBCs located at the tertiary amines to the LUMO orbitals mainly located at the  $\text{CBr}_4$  (Figure 6). Furthermore, the major peaks of UV-Vis spectra are observed in the area ranging from 220 nm (TMEDA- $\text{CBr}_4$ ) to 312 nm (DBU- $\text{CBr}_4$ ), where also CT is observed from the tertiary amines to  $\text{CBr}_4$ . Finally, it should be noted that in both peaks (first peak and major peak), electron charge is also observed, along the Br $\cdots$ N bond (Table S3 and Figure 6). The Br $\cdots$ N bond distance of the XBCs not only affects the C–Br bond lengths, where elongated Br $\cdots$ N bond distances result in short C–Br bond lengths (Figure 7a), but also their UV-Vis absorption spectra (Figure 7b). If the halogen bond did not play a significant role in the XBCs, it would be expected that the first main peak of the complex, i.e., peak corresponding in smaller energies, will correspond to the main UV-Vis absorption peak of  $\text{CBr}_4$ , since it presents an absorption peak in lower energy than the peak of the free amines. However, the formation of the halogen bond significantly affects the UV-Vis peaks. The main peak of the tertiary amines corresponds to the 2<sup>nd</sup> main peak of the XBCs. Both peaks present the same pattern with all studied amines, while the formation of the XB results in an increase of the amine's peak by about 50 nm (Figure 7b compare black and cyan lines). The 1<sup>st</sup> main peak of the XBCs also retains the general shape of the main peak of the free tertiary amines. However, it is significantly red shifted by about 200 nm, due to superposition of the  $\text{CBr}_4$  absorption peak and it is red shifted on the average by about 140 nm with respect to  $\text{CBr}_4$ . The absorption peaks of XBCs with the largest  $\lambda$  values correspond to the complexes of DIPEA and DABCO, because their second peaks are in higher energy than the absorption peak of the  $\text{CBr}_4$  and thus the superposition is larger. Comparing these two,

however, the DABCO- $\text{CBr}_4$  calculated peak is more red shifted, because its halogen bond is shorter than the halogen bond in DIPEA- $\text{CBr}_4$  and thus, the effect of the halogen bond is smaller in the last one. To conclude, short halogen bonds and UV-Vis peak of the complex components in the same area will result in significant red shifts, compared to the other complexes. Elongated halogen bond or absorption peaks located in different areas will result in less red shift of the complexes peaks.

Regarding the calculations for the homolytic cleavage of the C–Br bond, as shown in Table 3, the bond-dissociation energies of the C–Br bond are notably lower, when  $\text{CBr}_4$  participates in the formation of XBCs, compared to the case when  $\text{CBr}_4$  is not a part of a XBC complex. We have also taken into consideration the case of nucleophilic attack of the acceptor's N atom to Br atom of  $\text{CBr}_4$ , leading to the adducts [Acceptor-Br]<sup>+</sup> and [CBr<sub>3</sub>]<sup>−</sup>, i.e., heterolytic cleavage. The corresponding calculating energies are also presented in Table 3. It is easily noted that homolytic cleavage is substantially favored and possible to happen in the process under UVA irradiation. Finally, broken symmetry DFT calculations were performed to examine the homolytic cleavage via open singlet states. The  $S_0$  geometries of the XBCs complexes remain the same as the  $S_0$  geometries obtained via the simple DFT calculations.

The formation of a CTC between an XB donor and an XB acceptor may be observed experimentally in the UV-Vis spectra by the appearance of a new band shifted to higher wavelengths, upon mixing the two components.<sup>[1c,d,3a]</sup> Thus the UV-Vis spectra of each tertiary amine (XB acceptor) and  $\text{CBr}_4$  (XB donor) alone and of mixtures of XB acceptor and  $\text{CBr}_4$  in 1:1 mole ratio, specifically 0.1 M:0.1 M, were recorded in ACN (5 mL). In the case of DABCO, the spectrum for the 1:1 mole ratio was recorded, but the components were at a concentration of 0.01 M:0.01 M, since at 0.1 M, DABCO formed crystal structures with  $\text{CBr}_4$  in accordance with literature.<sup>[6b]</sup> Figure 5 (right) depicts the UV-Vis spectra for the six pairs. In all cases, the addition of  $\text{CBr}_4$  into a solution of the tertiary amine clearly caused a red shift, indicating the formation of a CTC. These shifts are quite similar in all cases. In the cases of Et<sub>3</sub>N- $\text{CBr}_4$ , TMEDA- $\text{CBr}_4$  and DBU- $\text{CBr}_4$ , the new band formed was shifted

**Table 3.** Calculated bond-dissociation Gibbs energies (in kcal mol<sup>−1</sup>) for the C–Br bond homolytic cleavage of  $\text{CBr}_4$  and XBCs, and calculated energies for the case of nucleophilic substitution in ACN solvent at the  $\omega$ B97X-D/def2-TZVP level of theory.

$\text{CBr}_4$ or XBC	Homolytic cleavage of C–Br	Promoted C–Br cleavage	$\Delta$ (Homolytic)	Nucleophilic attack (heterolytic cleavage)
	$\Delta G$	$\Delta G$	$\Delta G$	$\Delta G$
$\text{CBr}_4$	41.0			
Et <sub>3</sub> N- $\text{CBr}_4$		16.0	25.0	71.6
TMEDA- $\text{CBr}_4$		19.9	21.1	77.9
DIPEA- $\text{CBr}_4$		16.1	24.9	77.9
NMM- $\text{CBr}_4$		18.1	22.9	77.5
DABCO- $\text{CBr}_4$		19.6	21.4	74.3
DBU- $\text{CBr}_4$		24.3	19.7	63.6

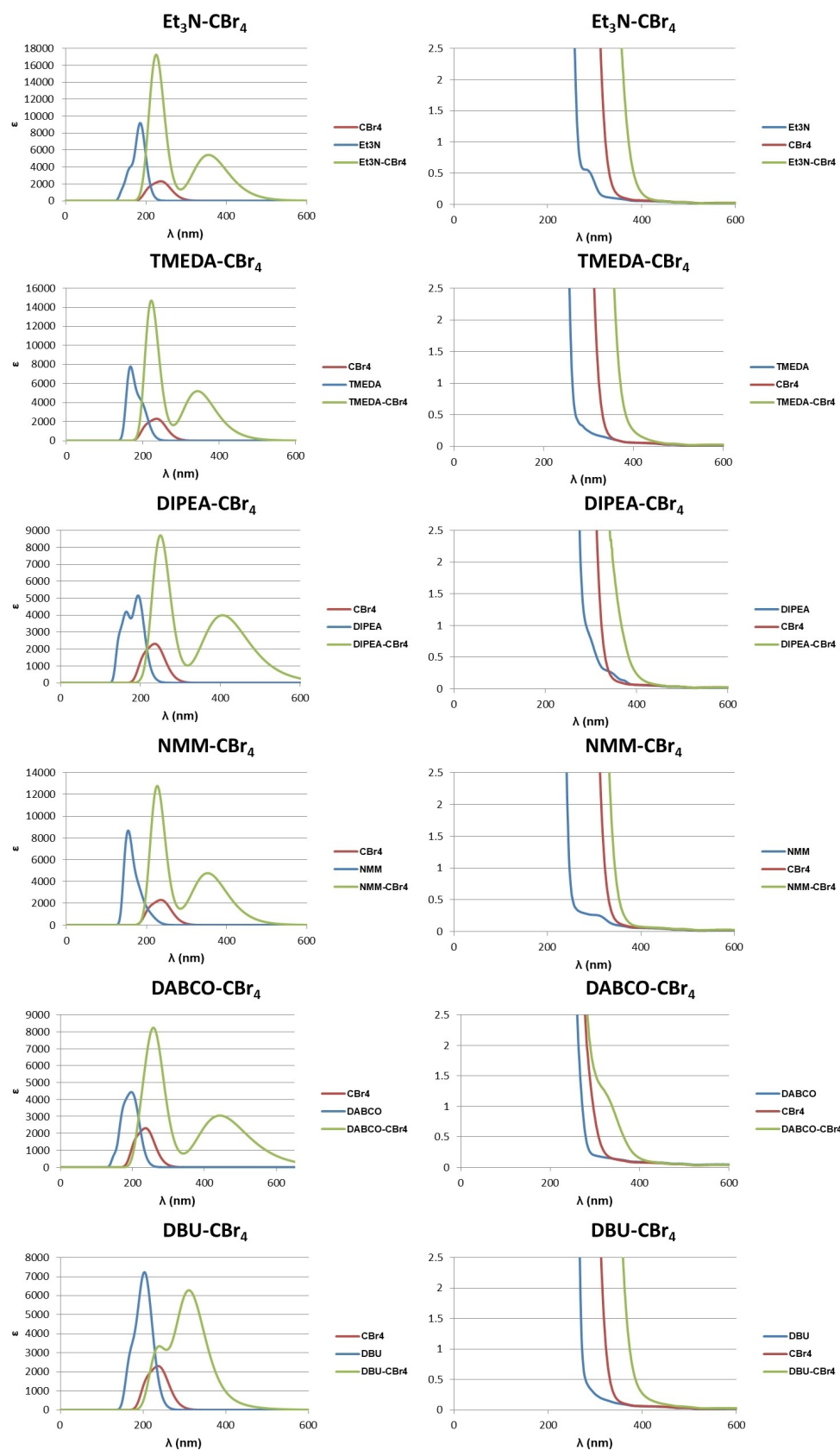


Figure 5. Calculated (TDA-B3LYP/def2-TZVP methodology, left) and experimental UV-Vis spectra (right) of the XBCs and their components in acetonitrile.

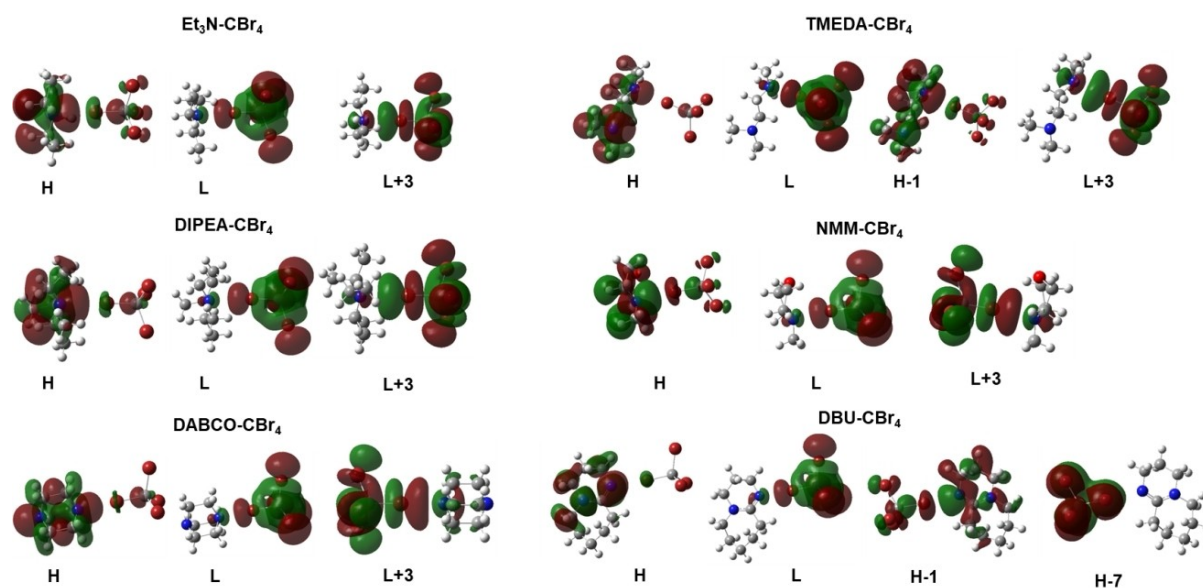


Figure 6. The calculated orbitals of the main excitations of the XBCs with the  $\omega$ B97X-D/def2-TZVP methodology.

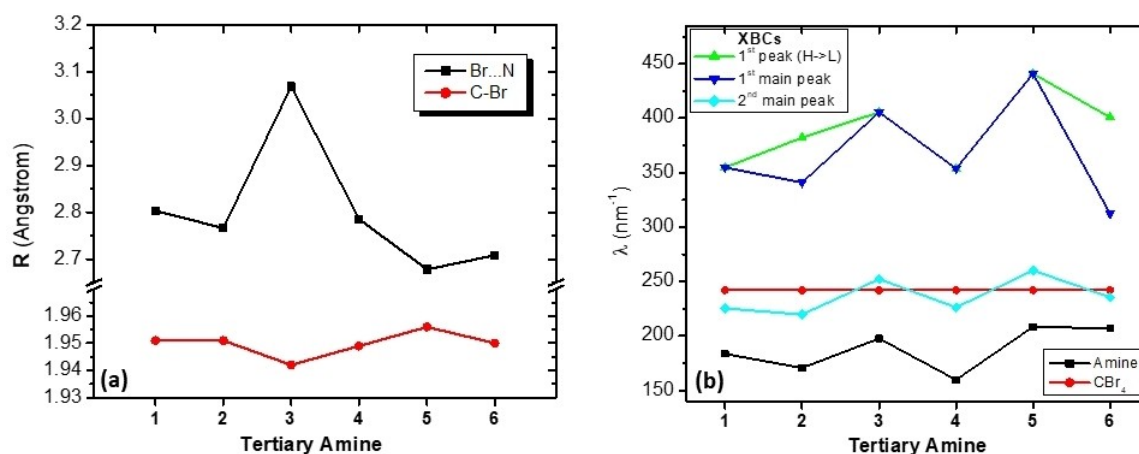


Figure 7. A) Calculated Br–N and C–Br bond lengths of XBCs with respect to the change of the amines, B)  $\lambda$  (nm) values of the main peaks of the amines, CBr<sub>4</sub>, and XBCs' absorption with respect to the change of the amines; 1: Et<sub>3</sub>N, 2: TMEDA, 3: DIPEA, 4: NMM, 5: DABCO, 6: DBU.

to 370–400 nm region, while for DIPEA-CBr<sub>4</sub> to 360–400 nm region. A smaller shift was observed for NMM-CBr<sub>4</sub>, where the new band was shifted to 340–380 nm region. In the case of DABCO, the new band is observed at 330–390 nm region. However, due to the fact that the concentration is substantially lower (0.01 M), it is expected to have a larger shift at slightly higher concentrations, probably exceeding the bands formed by the other complexes. Additional UV-Vis spectra of a series of solutions of Et<sub>3</sub>N-CBr<sub>4</sub>, TMEDA-CBr<sub>4</sub> and DABCO-CBr<sub>4</sub> were recorded, keeping the concentration of CBr<sub>4</sub> constant at  $3.0 \times 10^{-3}$  M, and are depicted in Figure S10 (Supporting Information).<sup>[17]</sup> Distinct absorption bands were observed for the XBCs in all cases, similarly to the work of Kochi *et al.*<sup>[6b]</sup> The above UV-Vis spectroscopic studies lead to a clear conclusion that all the studied tertiary amines form CTCs with CBr<sub>4</sub>, which may happen via formation of halogen bonds.

Furthermore, the experimental results seem to correlate quite fairly with the theoretical ones, supporting the methodology followed for the corresponding calculations. Additionally, UV-Vis spectra of DABCO and mixtures of DABCO-BrCCl<sub>3</sub>, DABCO-CCl<sub>4</sub> and DABCO-CH<sub>2</sub>Br<sub>2</sub> were recorded and the red shift observed indicated the formation of CTCs (Supporting Information).<sup>[17]</sup>

Several studies of XBC generation in solution have been performed employing NMR spectroscopy.<sup>[24]</sup> However, to our knowledge, no systematic study regarding tertiary amines and CBr<sub>4</sub> has been carried out so far. Thus, we investigated the interactions between the XB donors and CBr<sub>4</sub>, employing <sup>13</sup>C-NMR.<sup>[17]</sup> Initially, <sup>13</sup>C-NMR spectra of solutions consisting of a mixture of each particular amine with CBr<sub>4</sub> were recorded and compared to the <sup>13</sup>C-NMR spectrum of CBr<sub>4</sub> in CDCl<sub>3</sub> or C<sub>6</sub>D<sub>6</sub>, in order to observe the XBC formation. In the cases of Et<sub>3</sub>N, DIPEA and NMM complexes, the concentrations of the solutions,

**Table 4.**  $^{13}\text{C}$ -NMR (100 MHz,  $\text{CDCl}_3$  or  $\text{C}_6\text{D}_6$ ) shifts of  $\text{CBr}_4$  carbon upon mixing with tertiary amines.

Tertiary Amine	Entry	Concentration (M)	$\delta_{\text{C}}$ ppm before mix	$\delta_{\text{C}}$ ppm after mix	$\Delta$ ppm
$\text{Et}_3\text{N}$	1	0.10	−29.71	−29.50	0.21
	2	0.50	−29.68	−29.00	0.68
	3 <sup>[a]</sup>	0.50	−27.88	−26.22	1.66
	4	1.00	−29.61	−28.49	1.12
	5 <sup>[a]</sup>	1.00	−27.88	−25.18	2.60
TMEDA	6	0.10	−29.71	−29.44	0.27
	7	0.20	−29.70	−29.07	0.63
	8 <sup>[a]</sup>	0.20	−27.90	−25.29	2.61
DIPEA	9	0.10	−29.71	−29.72	0.01
	10	0.50	−29.68	−29.62	0.06
	11 <sup>[a]</sup>	0.50	−27.88	−27.79	0.06
	12	1.00	−29.61	−29.52	0.09
	13 <sup>[a]</sup>	1.00	−27.88	−27.79	0.09
NMM	14	0.10	−29.71	−29.43	0.28
	15	0.50	−29.68	−28.72	0.96
	16 <sup>[a]</sup>	0.50	−27.88	−25.80	2.08
	17	1.00	−29.61	−28.30	1.31
	18 <sup>[a]</sup>	1.00	−27.88	−24.97	2.91
DABCO	19	0.10	−29.71	−28.90	0.81
	20	0.20	−29.70	−28.37	1.33
DBU	21	0.10	−29.71	−29.42	0.29
	22	0.20	−29.70	−29.17	0.53

[a] Samples recorded in  $\text{C}_6\text{D}_6$ .

whose NMR spectra were recorded, were 0.10 M, 0.50 M, and 1.00 M (Molarity), while in the cases of DABCO, TMEDA and DBU were 0.10 M and 0.20 M, due to insolubility of those mixtures at higher concentrations. Table 4 summarizes the observed chemical shifts for the  $\text{CBr}_4$  carbon atom.

According to the recorded NMR spectra, it is clear that formation of the XBCs between the studied tertiary amines and  $\text{CBr}_4$  could be observed via  $^{13}\text{C}$ -NMR spectroscopy. Furthermore, higher concentrations of the XBCs components lead to higher shifts, which are correlated with complex formation. Especially, when  $\text{Et}_3\text{N}$  or NMM or DABCO were mixed with  $\text{CBr}_4$ , higher shifts that exceeded 1.00 ppm were recorded in  $\text{CDCl}_3$  (1.12 ppm, 1.31 and 1.33 ppm, respectively, entries 4, 17 and 20, Table 4). The shifts observed for TMEDA (entries 6 and 7, Table 4) and DBU (entries 21 and 22, Table 4) complexes were quite similar, while the shifts for mixtures consisting of DIPEA and  $\text{CBr}_4$  were small to negligible (entries 9 to 13, Table 4). Since the selection of the solvent could be critical for studying XBC by NMR spectroscopy,<sup>[1b]</sup>  $^{13}\text{C}$ -NMR spectra of the XBCs were recorded in  $\text{C}_6\text{D}_6$  at selected concentrations (entries 3, 5, 8, 11, 13, 16 and 18 Table 4). DABCO- $\text{CBr}_4$  and DBU- $\text{CBr}_4$  solutions were not recorded, due to insolubility in  $\text{C}_6\text{D}_6$ . It is obvious that higher shifts of the C atom of  $\text{CBr}_4$  are observed in  $\text{C}_6\text{D}_6$

compared to  $\text{CDCl}_3$ , meaning that XBC generation is more favored. DIPEA- $\text{CBr}_4$  mixtures however exhibit the same behavior as in  $\text{CDCl}_3$ .

Subsequently, the association constants  $K_{\text{a}}$  of the DABCO- $\text{CBr}_4$ , DIPEA- $\text{CBr}_4$  and TMEDA- $\text{CBr}_4$  complexes were determined by using the NMR version of the Benesi-Hildebrand (Hanna-Ashbaugh) method<sup>[25]</sup> (for details and graphs, see Supporting Information).<sup>[17]</sup> The experimental association constants and  $\Delta G_{\text{form}}$  are listed in Table 5. Comparing our experimental  $\Delta G_{\text{form}}$  values (Table 5) with the computed (Table 1), there is a difference of 2 kcal/mol in all cases. This results from the fact that in calculations, we have one XBC pair in solution, while experimentally, there are additional molecules of amines and  $\text{CBr}_4$ . Thus, in the experiment there is a dynamical equilibrium where

**Table 5.** Experimental association constants ( $K_{\text{a}}$ ) and  $\Delta G_{\text{form}}$  (kcal mol<sup>−1</sup>) of selected XBCs in  $\text{CDCl}_3$  (T = 298.15 K).

XBC	$K_{\text{a}}$	$\Delta G_{\text{form}}$
DABCO- $\text{CBr}_4$	0.57	0.3
DIPEA- $\text{CBr}_4$	0.06	1.7
TMEDA- $\text{CBr}_4$	0.52	0.4

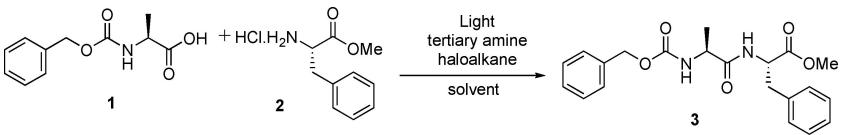


all molecules can interchange their pair partner and thus weaken the interaction that can be measured via NMR experiments.

According to the acquired results, the formation of the XBCs is an endergonic process, supporting the initial computational approach. DIPEA- $\text{CBr}_4$  seems to have a much smaller  $K_a$  (0.06) compared to the DABCO- $\text{CBr}_4$  and TMEDA- $\text{CBr}_4$  complexes (0.57 and 0.52, respectively, Table 5). Both complexed and uncomplexed forms are evident in all cases. The experimental  $\Delta G_{\text{form}}$  of the DABCO- $\text{CBr}_4$  and TMEDA- $\text{CBr}_4$  complexes are close enough, just like the computational results showcased. It should be noted that the acquired  $K_a$  of the DABCO- $\text{CBr}_4$  complex is much lower than the value reported by Kochi *et al.*,<sup>[6b]</sup> under conditions of excess of DABCO via UV-Vis spectroscopy (vs NMR in this work). The above results suggest that  $^{13}\text{C}$ -NMR spectroscopy indeed enables the identification of interactions, such as halogen bonding.

Having established both computationally and spectroscopically that various tertiary amines are able to form XBCs with  $\text{CBr}_4$ , we explored the ability of such complexes to initiate a synthetic application, such as the amino acid coupling. To this end, we studied the photochemical coupling of carbobenzoxy-L-alanine (Z-Ala-OH, 1) to methyl phenylalaninate (H-Phe-OMe, 2), using various tertiary amines as XB acceptors and  $\text{CBr}_4$  as an XB donor, under light irradiation (Table 6). Ten equivalents of tertiary amine and  $\text{CBr}_4$  and two equivalents of the amine component were used in all cases. In most cases, acetonitrile was employed as the solvent and the duration of irradiation was 6 hours. The results are summarized in Table 6. Initially, we checked the amino acid coupling using DMAP and  $\text{CBr}_4$ . Under LED 370 nm irradiation, the product was obtained in 75 % yield after 6 h and in 77 % yield after 18 h (entries 1 and 2, Table 6), while under sunlight irradiation for 8 h, the yield of 3 was 68 % (entry 3, Table 6). When  $\text{Et}_3\text{N}$  and TMEDA were used as tertiary amines, the product was isolated in lower yields (41 % and 32 %, respectively).

**Table 6.** Photochemical coupling of Z-L-Ala-OH (1) to HCl.H-Phe-OMe (2) using a tertiary amine and  $\text{CBr}_4$ .<sup>[a]</sup>

						
Entry	Haloalkane/equivalents	Tertiary amine/equivalents	Solvent	Light (nm)	Time (h)	Yield (%) <sup>[b]</sup>
1	$\text{CBr}_4/10$	DMAP/10	ACN	370	6	75
2	$\text{CBr}_4/10$	DMAP/10	ACN	370	18	77
3	$\text{CBr}_4/10$	DMAP/10	ACN	sunlight	8	68
4	$\text{CBr}_4/10$	$\text{Et}_3\text{N}/10$	ACN	370	6	41
5	$\text{CBr}_4/10$	TMEDA/10	ACN	370	6	32
6	$\text{CBr}_4/10$	DIPEA/10	ACN	370	6	53
7	$\text{CBr}_4/5$	DIPEA/5	ACN	370	6	19
8	$\text{CBr}_4/10$	NMM/10	ACN	370	6	46
9	$\text{CBr}_4/10$	DBU/10	ACN	370	6	19
10	$\text{CBr}_4/10$	DABCO/10	ACN	370	6	72
11	$\text{BrCCl}_3/10$	DABCO/10	ACN	370	6	51
12	$\text{CCl}_4/10$	DABCO/10	ACN	370	6	52
13	$\text{CH}_2\text{Br}_2/10$	DABCO/10	ACN	370	6	1
14	$\text{CBr}_4/5$	DABCO/5	ACN	370	6	46
15	$\text{CBr}_4/10$	DABCO/10	DCE	370	6	71
16	$\text{CBr}_4/10$	DABCO/10	ACN	370	18	79
17	$\text{CBr}_4/10$	DABCO/10	ACN	sunlight	8	65
18	$\text{CBr}_4/10$	DABCO/10	ACN	390	18	72
19	$\text{CBr}_4/10$	DABCO/10	ACN	427	18	67
20	$\text{CBr}_4/10$	DABCO/10	ACN	440	18	67
21	$\text{CBr}_4/10$	DABCO/10	ACN	456	18	68
22	$\text{CBr}_4/10$	DABCO/10	ACN	467	18	75
23	$\text{CBr}_4/10$	DABCO/10	ACN	525	18	12
24	$\text{CBr}_4/10$	DABCO/10	ACN	dark	18	–

[a] Reaction conditions: 1 (0.28 mmol), 2 (0.56 mmol), tertiary amine (2.84 mmol), haloalkane (2.84 mmol), ACN or DCE (4.25 mL), light irradiation at r.t.  
[b] Yield of 3 after isolation by column chromatography.

respectively, entries 4 and 5, Table 6). An attempt to decrease the equivalents of DIPEA from 10 to 5 led to a significant drop of the yield (entry 7, Table 6), which is in agreement with the results of DMAP- $\text{BrCCl}_3$ .<sup>[10d]</sup> NMM and DBU led to a moderate (46%) and a poor yield (19%) of the coupling product, respectively (entries 8 and 9, Table 6). Interestingly, the pair DABCO- $\text{CBr}_4$  provided **3** in 72% yield, after irradiation under LED 370 nm for 6 h (entry 10, Table 6). Since DABCO seemed to work well for the coupling reaction, we decided to extend our study using other halomethanes, instead of  $\text{CBr}_4$  along with DABCO. Using DABCO- $\text{BrCCl}_3$  under similar conditions, a significantly lower yield (51%) was achieved (entry 11, Table 6). DABCO- $\text{CCl}_4$  led to 52% yield (entry 12, Table 6), while DABCO- $\text{CH}_2\text{Br}_2$  practically did not provide the coupling product (entry 13, Table 6), suggesting that DABCO- $\text{CBr}_4$  is the optimum pair for the coupling reaction. An attempt to reduce the equivalents of DABCO and  $\text{CBr}_4$  from 10 to 5 led to a significant decrease of the yield (46%, entry 14, Table 6). Replacing ACN with 1,2-dichloroethane (DCE) as the solvent led to a similar yield (71%) under the same conditions (entry 15, Table 6). Extension of the reaction time from 6 h to 18 h resulted in an increased yield (79%, entry 16, Table 6). Finally, when the reaction was carried out under sunlight for 8 h (Athens, Greece, 37.97° N, 23.72° E), the product was isolated in 65% yield (entry 17, Table 6). As noticed, using either DABCO- $\text{CBr}_4$  or DMAP- $\text{CBr}_4$  under sunlight irradiation, similar yields were recorded (65% and 68%, respectively) (entries 17 and 3, Table 6). Due to seasonal limitations, continuous sunlight irradiation for more than 8 h was not feasible.

Although sunlight is a highly attractive zero-cost irradiation source, LED lamps serve as a low-cost irradiation source, which offers reliable and reproducible experimental results, overcoming seasonal and geographical limitations. While the reaction smoothly progresses under 370 nm, we explored the effect of higher wavelengths on the reaction outcome. In this context, where the individual starting materials do not exhibit absorption, the crucial role of the XBC in facilitating the reaction becomes more evident. To facilitate this investigation, we executed the reaction under optimal conditions, involving the use of 10 equivalents of  $\text{CBr}_4$  and DABCO with irradiation for 18 hours, employing a wide spectrum of different wavelengths between 370–525 nm (entries 16, 18–23, Table 6). Irradiation of the protected amino acids within the range of 390–456 nm resulted in comparable yields, ranging from 67–72% (entries 18–21, Table 6), albeit slightly lower than the optimal conditions at 370 nm. Of particular significance is the observation that performing the reaction under 467 nm yielded a 75% product formation (entry 22, Table 6), emphasizing the essential role of complex formation for the success of the reaction. Lastly, a noteworthy decrease in the reaction yield (12%) was observed when employing a 525 nm wavelength (entry 23, Table 6). These results align with our expectations, as longer wavelengths, such as 525 nm, typically results in reduced absorption by most compounds. The photochemical nature of the reaction was further accentuated by the absence of product formation when conducted under dark, as indicated in entry 24 of Table 6.

Recently, we have shown that Direct Infusion-High Resolution Mass Spectrometry<sup>[26]</sup> (DI-HRMS) is a powerful tool to study the reaction mechanism of light-mediated transformations.<sup>[11–13,27]</sup> Thus, in the present work, we explored the intermediates formed using the various pairs of tertiary amine- $\text{CBr}_4$  employing DI-HRMS. Initially, we monitored the course of the activation of Z-Ala-OH under irradiation at 370 nm of its mixture with DMAP- $\text{CBr}_4$ . We identified ions that may be attributed to the generation of DMAP-*N*-bromide **I<sub>a</sub>**, DMAP iminium ion **II<sub>a</sub>**, as well as the adduct of DMAP to iminium ion **III<sub>a</sub>** (Figure 8). In addition, ions corresponding to a hemiaminal ester of Z-Ala-OH **IV<sub>a</sub>** and alcohol **V<sub>a</sub>** were observed (Figure 8). Then, we monitored the course of the activation of Z-Ala-OH under irradiation at 370 nm of its mixture with DABCO- $\text{CBr}_4$ . As shown in Figure 8, ions corresponding to similar intermediates **I<sub>b</sub>**, **II<sub>b</sub>**, **III<sub>b</sub>**, **IV<sub>b</sub>** and **V<sub>b</sub>** were recorded.

HRMS data for the intermediates observed, when each one of the tertiary amines  $\text{Et}_3\text{N}$ , TMEDA, DIPEA, NMM or DBU were used in combination with  $\text{CBr}_4$  are presented in Supporting Information.<sup>[17]</sup> As we have presented in Table 6, the coupling using these tertiary amines was not so efficient, as in the case of DMAP or DABCO, leading to lower yields of the isolated product. However, for all the tertiary amine- $\text{CBr}_4$  pairs, similar ions were observed. Based on the HRMS data presented above, we may propose a general mechanism for the photoactivation of a carboxylic acid in the presence of a mixture of a tertiary amine- $\text{CBr}_4$ . Initially, an XBC is formed by mixing a tertiary amine with  $\text{CBr}_4$  (Scheme 1). Photoactivation of XBC by irradiation leads to the generation of *N*-brominated tertiary amine **I**, which by elimination of HBr provides iminium ion **II**. This is in equilibrium with adduct **III**, formed by nucleophilic attack of the tertiary amine onto **II**. Both **II** and **III** may lead to hemiaminal ester **IV**, upon reaction with the carboxylate component. The final amide product is formed after the nucleophilic attack of the amine component to **IV**.

## Conclusions

In conclusion, the present detailed studies indicate that a variety of tertiary amines may indeed serve as XB acceptors and form XBCs by interacting with  $\text{CBr}_4$  in solution. The results from the DFT calculations were consistent with the theoretical background of the halogen bonding as they confirmed its features, such as the linearity of the N–Br–C angle, the elongation of the C–Br bond of  $\text{CBr}_4$  and the shortening of the interatomic distance of N–Br below the sum of their vdW radii. The strongest binding energy was calculated for the DABCO- $\text{CBr}_4$  complex at –6.6 kcal/mol, which is stronger than a typical hydrogen bond in amines of –3.2 kcal/mol.<sup>[28]</sup> Spectroscopic studies, specifically computational and experimental UV-Vis studies and NMR experiments, confirmed the formation of XBCs and explained the shape of the absorption spectra. We conclude that short halogen bonds and UV-Vis peak of a complex's components in the same area will result in significant red shifts, compared to the other complexes. Elongated

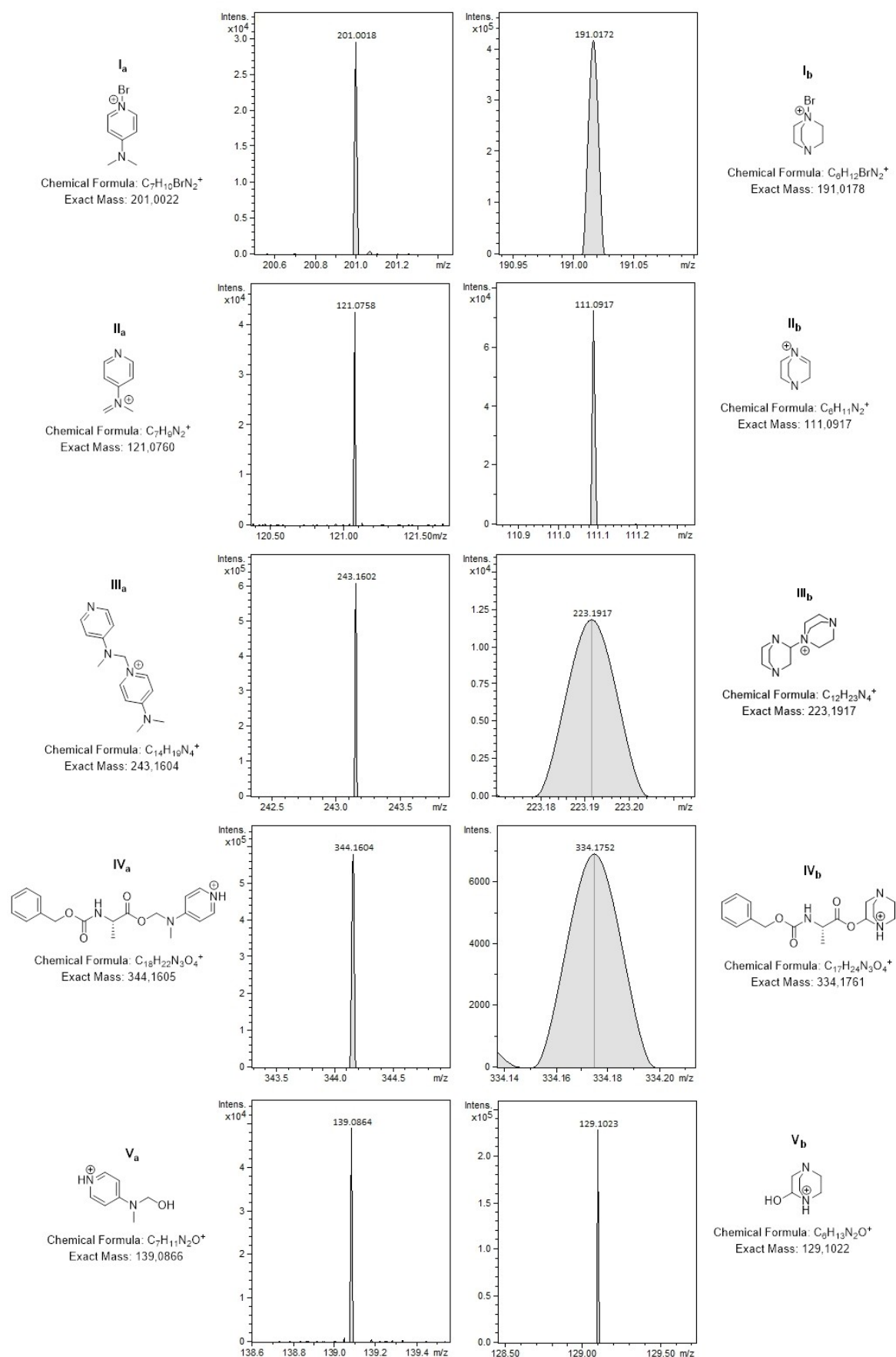
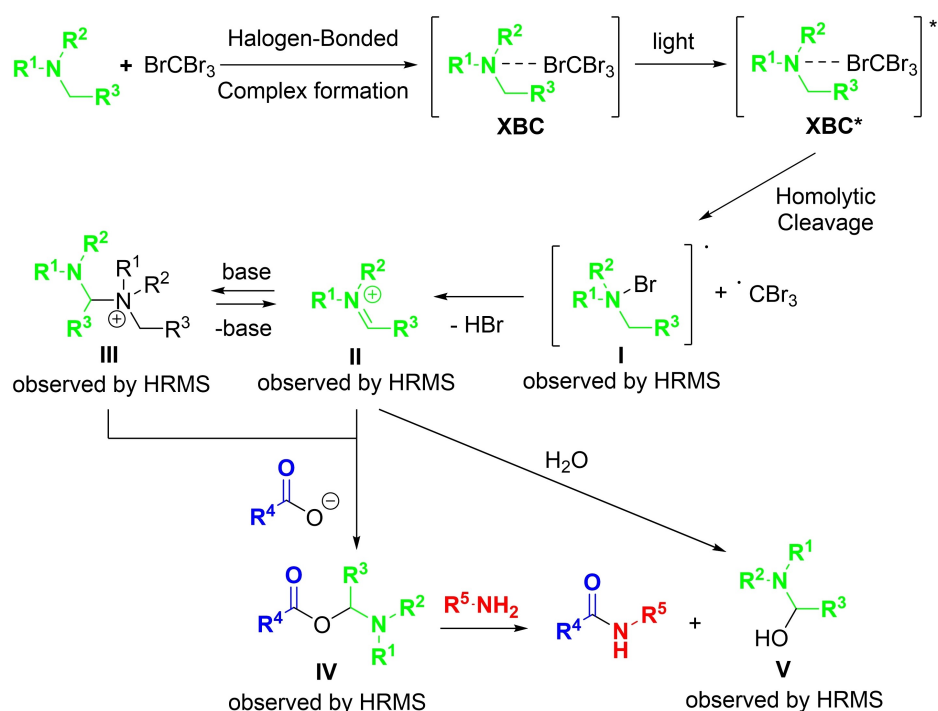


Figure 8. Selected HRMS data for the photoactivation of Z-Ala-OH using DMAP- $CBr_4$  and DABCOC $CBr_4$ .



**Scheme 1.** HRMS-guided general mechanism for light-mediated amide bond formation using a tertiary amine- $CBr_4$ .

halogen bond or absorption peaks located in different areas will result in less red shift of the complexes' peaks. Regarding the light-mediated amide formation, DABCO- $CBr_4$  seems to work well under either UVA irradiation or sunlight. Notably, the product was obtained in high yield (75%) under LED 467 nm irradiation, while slightly lower yields were achieved, when the reaction was performed under 390–456 nm irradiation. DI-HRMS studies revealed a general mechanism for all the XB donor-acceptor pairs as means to activate a carboxylic acid under irradiation and subsequently lead to amide synthesis. The mechanism starts with the *N*-bromination of the base, followed by the generation of an iminium ion and an adduct of the base to the iminium ion. The key carboxylic acid intermediate seems to be a hemiaminal ester, which after nucleophilic attack by an amine component leads to the final amide. The generality of the reaction mechanism, revealed by HRMS studies, may inspire further photochemical organic transformations. Thus, XBCs generated by a tertiary amine and  $CBr_4$  may find additional applications in photochemical organic transformations.

## Experimental Section

**General Procedure for the Light-mediated Coupling of Z-L-Ala-OH to HCl.H-Phe-OMe Using a Tertiary Amine and Halomethane  $CBr_4$ .** In a 25 mL Schlenk tube equipped with a PTFE-coated stirring bar, Z-L-Ala-OH (64 mg, 0.284 mmol), HCl.H-Phe-OMe (123 mg, 0.568 mmol), tertiary amine (2.84 mmol) and  $CBr_4$  (942 mg, 2.84 mmol) along with ACN (4.25 mL, HPLC grade) were added. The reaction mixture was stirred under light irradiation (Kessil lamps 370, 390, 427, 440, 456, 467, or 525 nm, sunlight and dark conditions) for 6 or 18 h. Then, the solvent was removed *in*

*vacuo* and the crude reaction mixture was treated with aqueous citric acid 10% (10 mL), before it was extracted with  $CH_2Cl_2$  ( $3 \times 10$  mL). The combined organic layers were washed with  $H_2O$  (10 mL), aqueous  $NaHCO_3$  (10 mL) and brine (10 mL), dried over  $Na_2SO_4$ , filtered and concentrated under reduced pressure. The desired product was purified by column chromatography.

**General Procedure for the Study of the Light-mediated (LED 370 nm) Generation of Intermediates from Z-Ala-OH Using a Tertiary Amine and  $CBr_4$ .** The generation of intermediates upon irradiation of a mixture of Z-Ala-OH with a tertiary amine and  $CBr_4$  with Kessil LED 370 nm were monitored for 3 hours by DI-HRMS. A tertiary amine (2.84 mmol),  $CBr_4$  (942 mg, 2.84 mmol) and Z-Ala-OH (64 mg, 0.284 mmol) were dissolved in ACN (4.25 mL) and the mixture was left stirring under irradiation at 370 nm at room temperature. At the specific time of study, a sample of the reaction mixture (20  $\mu$ L) was first diluted with 980  $\mu$ L ACN and 100  $\mu$ L of that sample were further diluted with 900  $\mu$ L of ACN. Finally, 100  $\mu$ L were directly injected to the ESI source of Q-TOF for analysis.

## Computational Details

Density functional theory (DFT) was used to calculate the binding energies between XB donors and acceptors in the XBCs. The geometries of the  $S_0$  and  $T_1$  states of all minima structures and the lowest in energy doublet states of the involved radicals were optimized. All calculations were carried out at the  $\omega$ B97X-D<sup>[15]</sup>/def2-TZVP<sup>[16]</sup> level of theory in acetonitrile solvent employing the default polarizable continuum solvent model PCM, which uses the integral equation formalism variant (IE-FPCM).<sup>[29]</sup> The used  $\omega$ B97X-D functional is appropriate for the calculation of both short- and long-range



interactions such as the halogen-bonding.<sup>[15]</sup> The frequencies of all optimized structures in  $S_0$  and in  $T_1$  states were computed, to calculate enthalpies and free energies (Standard conditions,  $P = 1$  atm,  $T = 298.15$  K) and verify that the optimized structures correspond to minima (no imaginary frequencies). The expression  $RT \ln(1/22.4)$  is used, which is a correction with regard to the reference state changing from ideal gas to solution. It converts an 1 atm standard state to a 1 M solution standard state. Furthermore, for the case of TMEDA- $\text{CBr}_4$ , the B3LYP-D3,<sup>[19]</sup> PBE0<sup>[21]</sup> and M06-2X<sup>[20]</sup>/def2-TZVP methodologies were also employed. It was found that all functionals present the same minimum structure with similar geometries. The vertical excitation energies for the XBCs, were calculated employing the Time-Dependent DFT (TD-DFT),<sup>[22,30]</sup> TD- $\omega$ B97X-D/def2-TZVP. Furthermore, the UV-Vis spectra were calculated using the Tamm-Dancoff Approximation (TDA)<sup>[23]</sup> at the TDA-B3LYP/def2-TZVP// $\omega$ B97X-D/def2-TZVP methodology. Specifically, the lowest 20 singlet and 20 triplet states were calculated. In the case of TMEDA,  $\text{CBr}_4$ , and TMEDA- $\text{CBr}_4$ , their UV-Vis absorption spectra were calculated via the TD- $\omega$ B97X-D/def2-TZVP, TDA- $\omega$ B97X-D/def2-TZVP and TDA-B3LYP/def2-TZVP methodologies, (Figure S1, Supporting Information).<sup>[17]</sup> The TDA-B3LYP/def2-TZVP methodology was in excellent agreement with the fact that XB causes red shifts in the absorption spectra, thus, this methodology was used for the calculation of all compounds and complexes. All calculations were carried out using the Gaussian16 code.<sup>[31]</sup>

## Supporting Information

The authors have cited additional references within the Supporting Information.<sup>[32,33]</sup>

## Acknowledgements

The research presented was carried out within the framework of a Stavros Niarchos Foundation grant to the National and Kapodistrian University of Athens (G.K.). The authors gratefully acknowledge the Hellenic Foundation for Research and Innovation (H.F.R.I.), since this research project was supported by the Hellenic Foundation for Research and Innovation (H.F.R.I.) under the “1st Call for H.F.R.I. Research Projects to support Faculty Members & Researchers and the Procurement of High-cost research equipment grant” (grant number 655) (C.G.K.). The research work was supported by the Hellenic Foundation for Research and Innovation (H.F.R.I.) under the H.F.R.I. PhD Fellowship grant (Fellowship Number:1338) (O.G.M.) and under the 5th Call for PhD Fellowships (Fellowship Number: :19213) (E.A.R.).

## Conflict of Interests

The authors declare no conflict of interest.

## Data Availability Statement

The data that support the findings of this study are available in the supplementary material of this article.

**Keywords:** halogen bonding · amide bond formation · DFT calculations · NMR studies · DI-HRMS studies

- [1] For selected books and reviews, see: a) D. A. Decato, E. A. John, O. R. Berryman in *Halogen Bonding in Solution*, 1<sup>st</sup> Edition (S. Huber), Wiley-VCH, Germany, 2021; b) M. Erdélyi, *Chem. Soc. Rev.* **2012**, 41, 3547–3557; c) T. M. Beale, M. G. Chudzinski, M. G. Sarwar, M. S. Taylor, *Chem. Soc. Rev.* **2013**, 42, 1667–1680; d) G. Cavallo, P. Metrangolo, R. Milani, T. Pilati, A. Priimagi, G. Resnati, G. Terraneo, *Chem. Rev.* **2016**, 116, 2478–2601.
- [2] L. A. Santos, T. C. Ramalho, T. A. Hamlin, F. M. Bickelhaupt, *Chem. Eur. J.* **2022**, 29, e202203791.
- [3] For selected reviews and papers, see: a) D. Bulfield, S. M. Huber, *Chem. Eur. J.* **2016**, 22, 14434–14450; b) X. Sun, W. Wang, Y. Li, J. Ma, S. Yu, *Org. Lett.* **2016**, 18, 4638–4641; c) A. Postigo, *Eur. J. Org. Chem.* **2018**, 46, 6391–6404; d) R. Beniazza, L. Remisse, D. Jardel, D. Lastérouères, J.-M. Vincent, *Chem. Commun.* **2018**, 54, 7451–7454; e) R. L. Sutar, S. Huber, *ACS Catal.* **2019**, 9, 9622–9639; f) R. Miao, D. Wang, J. Xiao, J. Ma, D. Xue, F. Liu, Y. Fang, *Phys. Chem. Chem. Phys.* **2020**, 22, 10212–10218; g) M. C. Gimeno, R. P. Herrera, *Eur. J. Org. Chem.* **2020**, 9, 1057–1058; h) E. M. Galathri, T. J. Kuczmera, B. J. Nachtsheim, C. G. Kokotos, *Green Chem.* **2024**, 26, 825–831.
- [4] For a recent review, see: H. L. Piedra, C. Valdez, M. Plaza, *Chem. Sci.* **2023**, 14, 5545–5568.
- [5] For selected examples, see: a) I. Kazi, S. Guha, G. Sekar, *Org. Lett.* **2017**, 19, 1244–1247; b) J. Wu, W. Sun, X. Sun, H. G. Xia, *Green Chem.* **2006**, 8, 365–367; c) J. Tan, F. Liang, Y. Wang, X. Cheng, Q. Liu, H. Yuan, *Org. Lett.* **2008**, 10, 2485–2488; d) L. Zhang, Y. Luo, R. Fan, J. Wu, *Green Chem.* **2007**, 9, 1022–1025.
- [6] a) D. P. Stevenson, G. M. Coppinger, *J. Am. Chem. Soc.* **1962**, 84, 149–152; b) S. C. Blackstock, J. P. Lorand, J. K. Kochi, *J. Org. Chem.* **1987**, 52, 1451–1460; c) S. V. Linderman, J. Hecht, J. K. Kochi, *J. Am. Chem. Soc.* **2003**, 125, 11597–11606; d) S. V. Rosokha, I. S. Neretin, T. Y. Rosokha, J. Hecht, J. K. Kochi, *Heteroat. Chem.* **2006**, 17, 449–459; e) W. S. Zou, J. Han, W. J. Jin, *J. Phys. Chem. A* **2009**, 113, 10125–10132; f) Q. J. Shen, W. J. Jin, *Phys. Chem. Chem. Phys.* **2011**, 13, 13721–13729; g) S. V. Rosokha, E. Lukacs, J. T. Ritzert, A. Wasilewski, *J. Phys. Chem. A* **2016**, 120, 1706–1715; h) K. Matsuo, E. Yamaguchi, A. Itoh, *J. Org. Chem.* **2020**, 85, 10574–10583.
- [7] For selected reviews, see: a) J. S. Carey, D. Laffan, C. Thomson, M. T. Williams, *Org. Biomol. Chem.* **2006**, 4, 2337–2347; b) S. D. Roughley, A. M. Jordan, *J. Med. Chem.* **2011**, 54, 3451–3479; c) D. G. Brown, J. Boström, *J. Med. Chem.* **2016**, 59, 4443–4458; d) A. I. Alfano, H. Lange, M. Brindisi, *ChemSusChem* **2022**, 15, e202102708.
- [8] For selected reviews, see: a) S.-Y. Han, Y.-A. Kim, *Tetrahedron* **2004**, 60, 2447–2467; b) C. A. G. N. Montalbetti, V. Falque, *Tetrahedron* **2005**, 61, 10827–10852; c) A. El-Faham, F. Albericio, *Chem. Rev.* **2011**, 111, 6557–6602.
- [9] For reviews, see: a) B. Lu, W.-J. Xiao, J.-R. Chen, *Molecules* **2022**, 27, 517–558; b) J. Singh, A. Sharma, *New J. Chem.* **2022**, 46, 16220–16242.
- [10] a) H. Liu, L. Zhao, Y. Yuan, Z. Xu, K. Chen, S. Qiu, H. Tan, *ACS Catal.* **2016**, 6, 1732–1736; b) W. Song, K. Dong, M. Li, *Org. Lett.* **2020**, 22, 371–375; c) V. Srivastava, P. K. Singh, P. P. Singh, *Tetrahedron Lett.* **2019**, 60, 40–43; d) A. K. Mishra, G. Parvari, S. K. Santra, A. Bazylevich, O. Dorfman, J. Rahamim, Y. Eichen, A. M. Szpilman, *Angew. Chem. Int. Ed.* **2021**, 60, 12406–12412; e) Y.-Q. Miao, J.-X. Kang, Y.-N. Ma, X. Chen, *Green Chem.* **2021**, 23, 3595–3599; f) J. Su, J.-N. Mo, X. Chen, A. Umanzor, Z. Zhang, K. N. Houk, J. Zhao, *Angew. Chem. Int. Ed.* **2022**, 61, e202112668.
- [11] A. Bourboulia, O. G. Mountanea, G. Krasakis, C. Mantzourani, M. G. Kokotou, C. G. Kokotos, *Eur. J. Org. Chem.* **2023**, 26, e202300008.
- [12] O. G. Mountanea, C. Mantzourani, M. G. Kokotou, C. G. Kokotos, G. Kokotos, *Eur. J. Org.* **2023**, 26, e202300046.
- [13] O. G. Mountanea, D. Psathopoulou, C. Mantzourani, M. G. Kokotou, E. A. Routsis, D. Tzeli, C. G. Kokotos, G. Kokotos, *Chem. Eur. J.* **2023**, 29, e2023005.
- [14] a) D. Cinčić, T. Friščić, W. Jones, *Chem. Eur. J.* **2008**, 14, 747–753; b) K. Raatikainen, K. Rissanen, *CrystEngComm* **2011**, 13, 6972–6977; c) A. A.

- Isse, C. Y. Lin, M. L. Coote, A. Gennaro, *J. Phys. Chem. B* **2011**, *115*, 678–684; d) L. Catalano, S. Perez-Estrada, H.-H. Wang, A. J.-L. Ayitou, S. I. Khan, G. Terraneo, P. Metrangolo, S. Brown, M. A. Garcia-Garibay, *J. Am. Chem. Soc.* **2017**, *139*, 843–848; e) C. Weinberger, R. Hines, M. Zeller, S. V. Rosokha, *Chem. Commun.* **2018**, *54*, 8060–8063; f) E. Adeniyi, O. Grounds, Z. Stephens, M. Zeller, S. V. Rosokha, *Molecules* **2022**, *27*, 6124.
- [15] J.-D. Chai, M. Head-Gordon, *Phys. Chem. Chem. Phys.* **2008**, *10*, 6615–6620.
- [16] F. Weigend, R. Ahlrichs, *Phys. Chem. Chem. Phys.* **2005**, *7*, 3297–3305.
- [17] For detailed results, computational and mechanistic studies, see Supporting Information.
- [18] C. E. Tzeliou, D. Tzeli, *J. Chem. Inf. Model.* **2022**, *62*, 6436–6448.
- [19] a) A. D. Becke, *J. Chem. Phys.* **1993**, *98*, 5648–5652; b) C. Lee, W. Yang, R. G. Parr, *Phys. Rev.* **1988**, *37*, 785–789; c) S. Grimme, J. Antony, S. Ehrlich, H. Krieg, *J. Chem. Phys.* **2010**, *132*, 154104.
- [20] Y. Zhao, D. G. Truhlar, *Theor. Chem. Acc.* **2008**, *120*, 215–241.
- [21] C. Adamo, V. Barone, *J. Chem. Phys.* **1999**, *110*, 6158–6169.
- [22] For selected examples, see; a) D. Tzeli, I. D. Petsalakis, G. Theodorakopoulos, *Phys. Chem. Chem. Phys.* **2011**, *13*, 11965–11975; b) D. Tzeli, G. Theodorakopoulos, I. D. Petsalakis, D. Ajami, J. Rebek Jr., *J. Am. Chem. Soc.* **2012**, *134*, 4346–4354; c) I. Skarmoutsos, D. Tzeli, I. D. Petsalakis, *J. Mol. Liq.* **2023**, *391*, 123220.
- [23] A. Chantzis, A. D. Laurent, C. Adamo, D. Jacquemin, *J. Chem. Theory Comput.* **2013**, *9*, 4517–4525.
- [24] For selected review and papers, see: a) R. D. Green, J. S. Martin, *J. Am. Chem. Soc.* **1968**, *14*, 3659–3668; b) J. F. Bertran, M. Rodriguez, *Org. Magn. Reson.* **1979**, *12*, 92–94; c) J. F. Bertran, M. Rodriguez, *Org. Magn. Reson.* **1980**, *14*, 244–246; d) J. F. Bertran, M. Rodriguez, *Org. Magn. Reson.* **1981**, *16*, 79–81; e) P. Metrangolo, W. Panzeri, F. Recupero, G. Resnati, *J. Fluorine Chem.* **2002**, *114*, 27–33; f) M. G. Sarwar, B. Dragisic, L. J. Salsberg, C. Gouliaras, M. S. Taylor, *J. Am. Chem. Soc.* **2010**, *132*, 1646–1653; g) D. V. D. Heiden, A. Vanderkooy, M. Erdélyi, *Coord. Chem. Rev.* **2020**, *407*, 213147.
- [25] For selected papers, see: a) H. A. Benesi, J. H. Hildebrand, *J. Am. Chem. Soc.* **1949**, *71*, 2703–2707; b) R. Mathur, E. D. Becker, R. B. Bradley, N. C. Li, *J. Phys. Chem.* **1963**, *67*, 2190; c) M. W. Hanna, A. L. Ashbaugh, *J. Phys. Chem.* **1964**, *68*, 811–816; d) Z. Meić, D. Vikić-Topić, R. Vuković, V. Kurešević, D. Fleš, *J. Pol. Sci.* **1981**, *19*, 3035–3037.
- [26] For selected reviews and papers, see: a) F. Bachle, J. Duschmale, C. Ebner, A. Pfaltz, H. Wennemers, *Angew. Chem. Int. Ed.* **2013**, *52*, 12619–12623; b) F. Bachle, I. Fleischer, A. Pfaltz, *Adv. Synth. Catal.* **2015**, *357*, 2247–2254; c) P. G. Iseneger, F. Bachle, A. Pfaltz, *Chem. Eur. J.* **2016**, *22*, 17595; d) N. Kaplaneris, C. Spyropoulos, M. G. Kokotou, C. G. Kokotos, *Org. Lett.* **2016**, *18*, 5800–5803; e) I. Triandafillidi, M. G. Kokotou, D. Lotter, C. Sparr, C. G. Kokotos, *Chem. Sci.* **2021**, *12*, 10191–10196; f) L. Wang, W. Lv, X. Sun, F. Zheng, T. Xu, X. Liu, H. Li, X. Lu, Xi. Peng, C. Hu, G. Xu, *Anal. Chem.* **2021**, *93*, 10528–10537; g) I. Perkons, J. Rusko, D. Zacs, V. Bartkevics, *Sci. Total Environ.* **2021**, *755*, 142688; h) M. G. Kokotou, *Curr. Pharm. Anal.* **2020**, *16*, 513–519; i) H. A. Haijes, M. Willemsen, M. van der Ham, J. Gerrits, M. L. Pras-Raves, H. C. M. T. Prinsen, P. M. van Hasselt, M. G. M. de Sain-van der Velden, N. M. Verhoeven-Duif, J. J. M. Jans, *Metabolites* **2019**, *9*, 12.
- [27] a) I. Triandafillidi, M. G. Kokotou, C. G. Kokotos, *Org. Lett.* **2018**, *20*, 36–39; b) C. S. Batsika, C. Koutsilieris, G. S. Koutoulougenis, M. G. Kokotou, C. G. Kokotos, *Green Chem.* **2022**, *24*, 6224–6231.
- [28] A. Malloum, J. Conrardie, *Comput. Theor. Chem.* **2021**, *1200*, 113236.
- [29] M. Cozi, G. Scalmani, N. Rega, V. Barone, *J. Chem. Phys.* **2002**, *117*, 43–54.
- [30] M. E. Casida, in *Recent Advances in Density Functional Theory*, World Scientific, Singapore, **1995**.
- [31] Gaussian 16, Revision A.03, M. J. Frisch, G. W. Trucks, H. B. Schlegel, G. E. Scuseria, M. A. Robb, J. R. Cheeseman, G. Scalmani, V. Barone, G. A. Petersson, H. Nakatsuji, X. Li, M. Caricato, A. V. Marenich, J. Bloino, B. G. Janesko, R. Gomperts, B. Mennucci, H. P. Hratchian, J. V. Ortiz, A. F. Izmaylov, J. L. Sonnenberg, D. Williams-Young, F. Ding, F. Lipparini, F. Egidi, J. Goings, B. Peng, A. Petrone, T. Henderson, D. Ranasinghe, V. G. Zakrzewski, J. Gao, N. Rega, G. Zheng, W. Liang, M. Hada, M. Ehara, K. Toyota, R. Fukuda, J. Hasegawa, M. Ishida, T. Nakajima, Y. Honda, O. Kitao, H. Nakai, T. Vreven, K. Throssell, J. A. Montgomery, Jr., J. E. Peralta, F. Ogliaro, M. J. Bearpark, J. J. Heyd, E. N. Brothers, K. N. Kudin, V. N. Staroverov, T. A. Keith, R. Kobayashi, J. Normand, K. Raghavachari, A. P. Rendell, J. C. Burant, S. S. Iyengar, J. Tomasi, M. Cossi, J. M. Millam, M. Klene, C. Adamo, R. Cammi, J. W. Ochterski, R. L. Martin, K. Morokuma, O. Farkas, J. B. Foresman, D. J. Fox, Gaussian, Inc., Wallingford CT, **2016**.
- [32] L. A. Curtiss, M. P. McGrath, J. P. Blaudeau, N. E. Davis, R. C. Binning, L. Radom, *J. Chem. Phys.* **1995**, *103*, 6104–6113.
- [33] B. Kaur, M. Kaur, N. Kaur, S. Garg, R. Bhatti, P. Singh, *J. Med. Chem.* **2019**, *62*, 6363–6376.

Manuscript received: February 12, 2024  
Revised manuscript received: May 4, 2024  
Accepted manuscript online: May 7, 2024  
Version of record online: June 7, 2024